A Preclinical Trial and Molecularly Annotated Patient Cohort Identify Predictive Biomarkers in Homologous Recombination–deficient Pancreatic Cancer

Yifan Wang[1,2], Jin Yong Patrick Park[1,2], Alain Pacis[1,3], Robert E. Denroche[4], Gun Ho Jang[4], Amy Zhang[4], Adeline Cuggia[1,2], Celine Domecq[1,2], Jean Monlong[5], Maria Raitses-Gurevich[6], Robert C. Grant[4,7], Ayelet Borgida[8], Spring Holter[8], Chani Stossel[6,9], Simeng Bu[1,2], Mehdi Masoomian[10], Ilinca M. Lungu[4], John M.S. Bartlett[4,10], Julie M. Wilson[4], Zu-Hua Gao[11], Yasser Riazalhosseini[5], Jamil Asselah[12], Nathaniel Bouganim[12], Tatiana Cabrera[13], Louis-Martin Boucher[13], David Valenti[13], James Biagi[14], Celia M.T. Greenwood[5,12,15,16], Paz Polak[17], William D. Foulkes[2,5], Talia Golan[6,9], Grainne M. O'Kane[4,7], Sandra E. Fischer[10], Jennifer J. Knox[7], Steven Gallinger[4,7], and George Zogopoulos[1,2]

ABSTRACT

Purpose: Pancreatic ductal adenocarcinoma (PDAC) arising in patients with a germline *BRCA1* or *BRCA2* (g*BRCA*) mutation may be sensitive to platinum and PARP inhibitors (PARPi). However, treatment stratification based on g*BRCA* mutational status alone is associated with heterogeneous responses.

Experimental Design: We performed a seven-arm preclinical trial consisting of 471 mice, representing 12 unique PDAC patient-derived xenografts, of which nine were g*BRCA* mutated. From 179 patients whose PDAC was whole-genome and transcriptome sequenced, we identified 21 cases with homologous recombination deficiency (HRD), and investigated prognostic biomarkers.

Results: We found that biallelic inactivation of *BRCA1*/*BRCA2* is associated with genomic hallmarks of HRD and required for cisplatin and talazoparib (PARPi) sensitivity. However, HRD genomic hallmarks persisted in xenografts despite the emergence of therapy resistance, indicating the presence of a genomic scar. We identified tumor polyploidy and a low Ki67 index as predictors of poor cisplatin and talazoparib response. In patients with HRD PDAC, tumor polyploidy and a basal-like transcriptomic subtype were independent predictors of shorter survival. To facilitate clinical assignment of transcriptomic subtype, we developed a novel pragmatic two-marker assay (GATA6:KRT17).

Conclusions: In summary, we propose a predictive and prognostic model of g*BRCA*-mutated PDAC on the basis of HRD genomic hallmarks, Ki67 index, tumor ploidy, and transcriptomic subtype.

Introduction

Pancreatic ductal adenocarcinoma (PDAC) is a difficult-to-treat malignancy with a 9% 5-year overall survival (1, 2). The inefficacy of unselected chemotherapy may reflect the molecular heterogeneity of PDAC. Recently, distinct genomic and transcriptomic subtypes of PDAC have been identified, and may inform treatment stratification (3–6). Five percent to 10% of incident PDAC cases are associated with germline loss-of-function mutations in *BRCA1, BRCA2*, or *PALB2* (7, 8). These genes are implicated in DNA damage response through homologous recombination repair (HRR; ref. 9).

We have previously shown *in vitro* that *BRCA1*- and *BRCA2*-mutated PDAC cell lines are sensitive to platinum and PARP inhibitors (PARPi; ref. 10). Platinums induce DNA interstrand cross-links, which leads to double-strand breaks (DSB) that cannot be effectively repaired by homologous recombination–deficient (HRD) cells (11). PARPis prevent the repair of single-strand breaks (SSB) through several mechanisms, including PARP trapping. As SSBs progress to DSBs, the accumulation of DNA damage is synthetic lethal in replicating HRD cells (12, 13).

Retrospective clinical series have suggested that patients with late-stage PDAC and a germline *BRCA1* or *BRCA2* (g*BRCA*) mutation may have a survival benefit with platinum-based treatment (7, 14–16). Recently, the POLO trial showed longer progression-free survival with maintenance olaparib (PARPi) in patients with platinum-sensitive g*BRCA*-mutated metastatic PDAC (17). However, 17% of g*BRCA*-mutated patients in this trial progressed on first-line platinum therapy, highlighting the heterogeneity in platinum responses. In g*BRCA*-mutated breast and ovarian cancer, the absence of biallelic *BRCA1* or

[1]Rosalind and Morris Goodman Cancer Research Centre of McGill University, Montreal, Quebec, Canada. [2]Research Institute of the McGill University Health Centre, Montreal, Quebec, Canada. [3]Canadian Centre for Computational Genomics, McGill University and Genome Quebec Innovation Center, Montreal, Quebec, Canada. [4]Ontario Institute for Cancer Research, Toronto, Ontario, Canada. [5]Department of Human Genetics, McGill University, Montreal, Quebec, Canada. [6]Pancreatic Cancer Translational Research Laboratory, Oncology Institute, Sheba Medical Center, Tel Hashomer, Ramat Gan, Israel. [7]Wallace McCain Centre for Pancreatic Cancer, Princess Margaret Cancer Centre, Toronto, Ontario, Canada. [8]Lunenfeld Tanenbaum Research Institute, Mount Sinai Hospital, Toronto, Ontario, Canada. [9]Sackler Faculty of Medicine, Tel Aviv University, Tel Aviv, Israel. [10]Department of Laboratory Medicine and Pathobiology, University of Toronto, Toronto, Ontario, Canada. [11]Department of Pathology, McGill University, Montreal, Quebec, Canada. [12]Department of Oncology, McGill University, Montreal, Quebec, Canada. [13]Department of Diagnostic Radiology, McGill University, Montreal, Quebec, Canada. [14]Department of Oncology, Queen's University, Kingston, Ontario, Canada. [15]Department of Epidemiology, Biostatistics and Occupational Health, McGill University, Montreal, Quebec, Canada. [16]Lady Davis Institute for Medical Research, Jewish General Hospital, Montreal, Quebec, Canada. [17]Icahn School of Medicine at Mount Sinai Hospital, New York, New York.

Note: Supplementary data for this article are available at Clinical Cancer Research Online (http://clincancerres.aacrjournals.org/).

Corresponding Author: George Zogopoulos, The Research Institute of the McGill University Health Centre, 1001 Decarie Blvd, Rm EM2.3210, Montreal, Quebec, H4A 3J1 Canada. Phone: 514-934-1934; E-mail: george.zogopoulos@mcgill.ca

Clin Cancer Res 2020;26:5462–76

doi: 10.1158/1078-0432.CCR-20-1439

Translational Relevance

Pancreatic cancers associated with a germline *BRCA1*/*BRCA2* (g*BRCA*) mutation may be targetable using DNA-damaging agents, such as platinum and PARP inhibitors. However, treatment stratification based on germline mutational status alone, and assumed homologous recombination deficiency (HRD), is associated with heterogeneous outcomes. In this study, we combine a multi-institutional patient cohort and a multiarm preclinical trial to identify biomarkers to guide treatment decisions. We propose a predictive and prognostic model of g*BRCA*-mutated pancreatic cancer on the basis of genomic hallmarks of HRD, Ki67 index, tumor ploidy, and transcriptomic subtype. Because the basal-like transcriptomic subtype is associated with worse survival, we propose a novel and clinically pragmatic IHC assay (GATA6:KRT17) to facilitate assignment of transcriptomic subtype.

BRCA2 inactivation has been implicated in primary resistance to platinum therapy (18). Reversion mutations that restore *BRCA1* or *BRCA2* function have been described as a mechanism of acquired resistance (19, 20). However, the majority of g*BRCA* tumors do not exhibit a reversion mutation at the time of disease relapse (21). Together, these observations highlight the need to identify predictive biomarkers, beyond germline mutational status, in g*BRCA*-mutated PDAC.

Here, we performed a multiarm preclinical trial using mouse xenograft models derived from patients with g*BRCA*-mutated PDAC to evaluate their response to platinum and talazoparib, a second-generation PARPi with speculated higher potency. We demonstrate that HRD genomic hallmarks are required for sensitivity to platinum and PARPi therapy, whereas tumor polyploidy predicts poor response to these therapies. Furthermore, by integrating clinical and molecular profiling data from 21 patients with HRD PDAC, we suggest that tumor polyploidy and a basal-like transcriptomic subtype are poor prognostic variables in HRD PDAC.

Materials and Methods

Patients

Patients with *gBRCA*-mutated PDAC were identified from three institutions: McGill University Health Centre (Montreal, Quebec, Canada), Princess Margaret Cancer Centre (Toronto, Ontario, Canada), and Chaim Sheba Medical Centre (Tel-Hashomer, Ramat Gan, Israel). Patients enrolled in the COMPASS molecular profiling trial (NCT02750657) from December 2015 to April 2019 were also included. Patient demographics, surgical procedure, chemotherapy treatment, and survival data were abstracted from prospectively maintained institutional research databases. Clinical staging was based on the 8th edition of the American Joint Committee on Cancer for PDAC. Survival was calculated from the initial date of pathologic diagnosis until death or censor date.

Germline sequencing of homologous recombination–proficient cases

Homologous recombination–proficient (HRP) cases included in the preclinical trial were identified by sequencing for germline mutations in HRD genes using a targeted panel of 710 cancer-related genes, including full gene sequencing of *BRCA1, BRCA2, PALB2*, and *ATM*. The targeted regions were captured using Agilent SureSelect Technology (Agilent Technologies). Samples were sequenced on the Illumina MiSeq Platform (Illumina Inc.) with 300-bp paired-end reads.

Whole-genome sequencing

Fresh frozen human and xenograft tumor tissues underwent laser capture microdissection for tumor cell enrichment prior to DNA extraction. Whole-genome sequencing (WGS) of tumor and matched lymphocyte DNA was performed at the Ontario Institute for Cancer Research (Toronto, Ontario, Canada) using established institutional pipelines (22). Germline and somatic variant calling, ploidy determination, and neoantigen quantification protocols have been described previously. HRDetect scores were calculated as described by Davies and colleagues (23). Mutational signature proportions were derived by applying a nonnegative least squares linear algorithm, as reported previously (24). All germline mutations and somatic hits were confirmed in xenografts by Sanger sequencing.

RNA sequencing

Xenograft tumor tissues were preserved in RNAlater, and disrupted and homogenized using the Qiagen TissueLyser II (Qiagen). RNA was extracted using the Qiagen RNeasy Plus Universal Mini Kit (Qiagen). Sequencing was performed by BGI Americas and the McGill University Genome Quebec Innovation Centre (Montreal, Quebec, Canada, MUGQIC). Libraries were sequenced on the Illumina HiSeq 2000 (BGI Americas) or HiSeq 2500 (MUGQIC) platforms with TruSeq V3 reagents, to generate 100-bp paired-end reads at a sequencing depth of 50×10^6 reads.

Adaptor sequences and low-quality score bases (Phred score < 30) were trimmed using Trimmomatic (25). The resulting reads were aligned to the human genome reference sequence (GRCh38/hg38), using STAR (26). To remove possible contaminated reads originating from mouse in xenograft samples, reads were also aligned to the GRCm38/mm10 mouse, and the Disambiguate algorithm (version 1.0; ref. 27) was used to assign reads to individual species based on the highest quality alignment of the read pair (Supplementary Fig. S1). Count data (originating from human reads) for each sample were obtained using HTSeq (28). For downstream analyses, we excluded lowly expressed genes with an average read count lower than 10 across all of the samples. Raw counts were normalized using the TMM algorithm (i.e., weighted trimmed mean of M-values), implemented in edgeR R package (version 3.22.5; ref. 29). Using the voom function in the limma R package (version 3.36.5; ref. 30), the data were converted to log-counts per million. The removeBatchEffect function from limma was used to correct for both batch effects. Heatmaps were constructed using unsupervised hierarchical clustering (ward.D2 method). Transcriptomic classification into classical and basal-like subtypes was performed as described by Moffitt and colleagues (3).

Establishment of patient-derived xenografts

Mice were housed in a pathogen-free facility, on a 12-hour light–dark cycle, with *ad lib* access to water and sterile rodent chow. Fresh PDAC tissue was obtained from the operating theater or interventional radiology suite, minced into 1 mm^3 pieces, and subcutaneously implanted into the flanks of 6- to 8-week-old female SCID beige mice (Charles River Laboratories). Xenografts were grown to 1 cm^3, harvested, and serially passaged into new SCID beige mice. Tumors were cryopreserved in FBS with 10% dimethyl sulfoxide.

Multiarm preclinical trial design

Fourth-passage patient-derived tumors were implanted into the right and left flanks of 6- to 8-week-old female SCID beige mice.

When the tumor volume reached 120 mm^3, mice were randomized to one of seven treatment arms with the goal of treating six to 10 mice per arm. The treatment arms were: (i) cisplatin (Enzo Life Sciences) 4 mg/kg, once weekly, intraperitoneal; (ii) talazoparib (AbMole Biosciences) 0.33 mg/kg, 5 days on/2 days off, oral gavage; (iii) cisplatin–talazoparib combination; (iv) gemcitabine (LC Laboratories) 100 mg/kg, twice weekly, intraperitoneal; (v) gemcitabine–cisplatin combination; (vi) gemcitabine–talazoparib combination; and (vii) vehicle (PBS) 5 days on/2 days off, oral gavage, and once weekly intraperitoneal. Because pilot experiments showed increased toxicity with talazoparib (Supplementary Fig. S2), we randomized at least 10 mice into the talazoparib arms, in anticipation that a greater fraction of mice in these arms may not complete the treatment course. Treatment was administered for 28 days, with half-dosing or skipped dosing, if mice lost >10% or >12.5% of their original weight, respectively. Mice were weighed, and tumors were measured by caliper twice weekly. Three mice in each treatment arm were sacrificed on day 29, and their tumors were collected and subjected to formalin fixation and paraffin embedding for histologic analyses. The survival of these mice was censored at day 29. The remaining mice were euthanized when the tumor volume exceeded 2 cm^3, or if they lost >20% of their original weight.

Tissue microarrays

Tissue microarrays were constructed using an automated Tissue Microarrayer (TMA Grand Master, 3DHistech). Freshly harvested patient-derived xenograft (PDX) tumors were fixed in 10% buffered formalin for 24 hours, and paraffin embedded. Tumor cores (2 mm diameter) were punched from each donor paraffin-embedded block on the basis of previously demarcated areas on a corresponding hematoxylin and eosin (H&E)-stained slide. Each individual patient was represented by two to three unique PDX cores originating from early-passage mice. Overall, 33 cores representing 12 unique HRD PDAC xenografts were prepared on a tissue microarray, which was sectioned at 4-μm thickness for subsequent IHC analyses.

Single-marker and multiplex immunostaining

Four-micrometer thick serial sections of tissue microarray and patient tumor blocks were cut for H&E staining and IHC analyses. IHC was performed using the Discovery Ultra Autostaining Platform (Ventana Medical Systems). Slides were incubated with a primary antibody, followed by the corresponding horseradish peroxidase–conjugated secondary antibody (OmniMap anti-mouse No. 760-4310 or OmniMap anti-rabbit No. 760-4311, Ventana Medical Systems), developed with 3,3′-diaminobenzidine (DAB), and counterstained with hematoxylin. Primary antibodies used were as follows: anti-Ki67 (30-9, Ventana Medical Systems, undiluted), anti-cleaved caspase-3 (Asp175, Cell Signaling Technology, 1:100), anti-CD8 (SP57, Ventana Medical Systems, undiluted), anti-pancytokeratin (AE1/AE3/PCK26, Ventana Medical Systems, undiluted), anti-GATA6 (D61E4, Cell Signaling Technology, 1:500), anti-KRT17 (17516-1-AP, Proteintech, 1:100), and anti-KRT81 (11342-1-AP, Proteintech, 1:50). Multiplex chromogenic IHC was also performed on the Discovery Ultra platform, using Chromogenic Detection Kits from Ventana Medical Systems (No. 750-124, DAB; No. 760-247, teal).

Image analyses

Immunostained slides were scanned using the Aperio ScanScope (Aperio Technologies) at 20 × magnification. For Ki67 immunostaining, five regions of interest were randomly selected for each tumor, and manually annotated to exclude stromal and necrotic areas by a technician blinded to treatment assignment. Ki67 immunostaining was quantified by digital analysis of positively stained nuclei using the Aperio ImageScope Software (Aperio Technologies). Cleaved caspase-3, GATA6, KRT17, and KRT81 immunostaining were quantified using the Halo (Indica Labs) Cytonuclear Algorithm (single marker) or multiplex IHC algorithm (multiplex IHC, mHIC). A tissue classifier was developed to automatically segment tumor from stroma and necrosis. Cell recognition and nuclear segmentation were optimized, and quality control was performed for each case.

H&E-stained sections were reviewed by a board-certified gastrointestinal pathologist (S.E. Fischer). Mitotic figures were counted manually, and expressed as the number of mitotic figures per 10 high-power fields.

Generation of primary cell cultures from HRD xenografts

Harvested xenograft tumors were mechanically minced, and underwent serial trypsin digestion at 37°C. Murine fibroblast contamination was eliminated by magnetic-activated cell sorting using the Miltenyi Mouse Cell Depletion Kit (ref. 31; Miltenyi Biotec). Cells were seeded on collagen-coated plates and cultured in RPMI supplemented with 10% FBS and 1% antibiotic/antimycotic solution, at 37°C in a humidified incubator with a 5% CO_2 atmosphere. Cell numbers were counted by trypan blue exclusion assay with a hematocytometer at 24-hour intervals for 7 days. Cell doubling times were calculated using a nonlinear regression (exponential growth equation) analysis.

Tumor ploidy determination

Q70P, Q70LM, and Q70AM primary cell lines were generated as described above. Cells were harvested by centrifugation, fixed with ethanol, and incubated in 0.5 mL cell-cycle buffer containing 30 μg/mL propidium iodide (PI, Sigma-Aldrich) and 50 μg/mL RNase A (Thermo Fisher Scientific). PI fluorescence data were collected from 10,000 cells on a flow cytometer, after gating to exclude dead cells, debris, and doublets (32). The Q70P cell line was used as a control to fix the voltage for the diploid population. DNA histograms were plotted using FlowJo (Tree Star Inc.).

To determine the ploidy of the HRP cases, genomic DNA was extracted from early-passage xenografts and SNP array was performed using the Illumina Infinium Omni2.5 Microarray. The allele-specific copy number analysis of tumors (ASCAT, v2.4.3) algorithm was used to infer tumor ploidy and tumor purity, as described previously (33). Each sample was run independently in "tumor-only" mode, using the "Illumina2.5M" profile within ASCAT. The ploidy estimates were compared across passages for each tumor.

Statistical analysis

Statistical analyses were performed using R Software, version 3.5 (R Foundation for Statistical Computing) and GraphPad Prism, version 6 (GraphPad). Differences between continuous variables were compared using the Wilcoxon rank-sum test. For forward stepwise multiple linear regression analysis, the criteria for entry into the model was $P < 0.1$ and for removal was $P > 0.15$. Overall survival was estimated using the Kaplan–Meier method and compared between treatment groups using a log-rank test. Hazard ratios were calculated using the Cox proportional hazards model. A $P < 0.05$ was considered statistically significant.

Study approval

This study was conducted in accordance with the principles of the Declaration of Helsinki. Use of human biospecimens and data were

approved by the local institutional review boards of each participating center. Patients provided written informed consent to participate. Animal studies were approved by the McGill University Animal Care Committee, and conducted in accordance with Animal Research: Reporting of *In Vivo* Experiments guidelines.

Results

Biallelic, but not monoallelic, *BRCA1* or *BRCA2* inactivation is associated with genomic hallmarks of HRD

Because biallelic inactivation of *BRCA1* or *BRCA2* has been associated with treatment responses in other cancer types, we performed WGS for seven unique g*BRCA*-mutated PDAC cases selected for the preclinical trial (Supplementary Table S1). Six of the seven samples showed biallelic loss of *BRCA1* ($n = 2$) or *BRCA2* ($n = 4$), due to LOH of the wild-type allele or a second somatic mutation. In contrast, the remaining sample (Q437) exhibited only a germline *BRCA2* mutation without a second somatic hit.

Tumors with biallelic *BRCA1* or *BRCA2* inactivation had higher HRDetect scores compared with the sample with monoallelic loss (>0.999 vs. 0.042; **Fig. 1A**). Biallelic inactivation cases exhibited a higher number of structural variants, driven by small deletions in the 100 bp–10 kbp range, consistent with rearrangement signature 5. They also displayed a single-nucleotide variant (SNV) burden that was dominated by COSMIC single-base substitution signature 3 (SBS3, 32.6% overall SNV), which is associated with defective HRR (34). In contrast, the case with monoallelic *BRCA2* inactivation had 0% SBS3 proportion. These findings suggest that biallelic, but not monoallelic, HR inactivation is associated with distinct mutational signatures, which are captured by a dominant SBS3 contribution and an elevated HRDetect score.

HRD PDAC xenografts are preferentially sensitive to cisplatin and talazoparib mono- and combination therapy

We evaluated 10 unique PDXs in a multiarm preclinical trial (387 mice in total) to evaluate their response to platinum, PARPi, and gemcitabine-based therapy. Of these 10 PDXs, six had biallelic *BRCA1* ($n = 2$) or *BRCA2* ($n = 4$) inactivation and genomic hallmarks of HRD as determined by WGS; these were considered HRD. The remaining xenografts had only monoallelic germline *BRCA2* loss ($n = 1$) or did not harbor a germline HR gene mutation ($n = 3$), and were considered HRP (Supplementary Table S1; Supplementary Fig. S3).

After 28 days of treatment, HRD xenografts showed a significantly greater treatment response to cisplatin monotherapy (2.50- vs. 4.97-fold change; $P < 0.001$), talazoparib monotherapy (2.35 vs. 5.73; $P = 0.003$), and cisplatin–talazoparib combination therapy (1.46 vs. 4.19; $P < 0.001$) compared with HRP xenografts (**Fig. 1B** and **C**). Gemcitabine monotherapy resulted in comparable tumor regression in both HRD and HRP xenografts (0.75 vs. 0.60; $P = 0.46$). Similarly, there was no difference in treatment response to combination gemcitabine–cisplatin or gemcitabine–talazoparib between HRD versus HRP xenografts.

Cisplatin–talazoparib combination resulted in greater tumor inhibition compared with talazoparib alone in both HRD (1.46 vs. 2.35; $P = 0.040$) and HRP xenografts (4.19 vs. 5.73; $P = 0.036$). In HRD xenografts, there was a trend toward improved efficacy with cisplatin–talazoparib compared with cisplatin alone (1.46 vs. 2.50; $P = 0.087$); however, no difference was seen for HRP xenografts (4.19 vs. 4.97; $P = 0.280$).

Gemcitabine–cisplatin is associated with prolonged survival in HRD PDAC xenografts

Because HRD and HRP xenografts had similar tumor regression following 28 days of gemcitabine mono- or combination therapy, we assessed differences in treatment durability. We compared the median overall survival (mOS) of mice in each treatment arm (gemcitabine vs. gemcitabine–cisplatin vs. gemcitabine–talazoparib) for HRD and HRP xenografts. Because mice were monitored until their tumor reached endpoint size, we used mOS as a surrogate for treatment durability. In mice bearing HRD tumors, gemcitabine–cisplatin was associated with significantly longer mOS compared with gemcitabine alone (126 vs. 106.5 days; $P = 0.048$) and gemcitabine–talazoparib (126 vs. 98 days; $P < 0.001$). There were no differences in mOS between gemcitabine alone and gemcitabine–talazoparib (106.5 vs. 98 days; $P = 0.14$). mOS was similar between all three treatment arms in HRP xenografts (**Fig. 1D** and **E**; Supplementary Fig. S4A and S4B).

Gemcitabine–talazoparib was the most toxic regimen, with 31% of mice euthanized prior to the end of treatment. This contrasts with the 9% and 0% on-treatment mortality in the gemcitabine–cisplatin and gemcitabine monotherapy arms, respectively. To adjust for regimen-related toxicity, we repeated the survival analyses including only those mice that completed 28 days of treatment. In HRD tumors, gemcitabine–cisplatin was again associated with longer mOS compared with gemcitabine alone (130 vs. 106.5 days; $P = 0.002$) and gemcitabine–talazoparib (130 vs. 109 days; $P = 0.020$). mOS was comparable between all three treatment arms for HRP tumors (Supplementary Fig. S4C and S4D).

Gemcitabine–cisplatin and gemcitabine–talazoparib suppress tumor proliferation in HRD xenografts

To investigate the antiproliferative effect of gemcitabine-based therapy, we evaluated the Ki67 index of PDXs at the end of treatment (day 29). HRD PDXs treated with gemcitabine–cisplatin (0.34 vs. 0.57; $P = 0.040$) and gemcitabine–talazoparib (0.23 vs. 0.60; $P < 0.001$) had a significantly lower relative Ki67 index compared with HRP tumors (**Fig. 2A** and **B**). With gemcitabine monotherapy also, HRD PDXs had a lower relative Ki67 index (0.38 vs. 0.63; $P = 0.161$), although this trend was not statistically significant. In addition, the Ki67 index was significantly correlated with mitotic activity across all PDXs ($R = 0.692$; $P < 0.001$; **Fig. 2C**). Furthermore, we evaluated cleaved caspase-3 immunostaining as a marker of apoptotic cell death. Gemcitabine–talazoparib was associated with significantly increased relative cleaved caspase-3 positivity in HRD versus HRP PDX (4.94 vs. 1.79; $P = 0.006$; Supplementary Fig. S5). Four cases (three HRD and one HRP) had minimal residual tumor at the end of treatment, and were insufficient for Ki67 and cleaved caspase-3 immunostaining.

Longitudinally derived HRD xenografts recapitulate the emergence of clinical chemoresistance

To study the evolution of treatment response to HRD-targeted therapies, we longitudinally derived three xenografts from a patient with biallelic *BRCA2*-mutated PDAC, over a 4.5-year disease course (**Fig. 3A** and **B**). The patient presented with a pancreatic tail PDAC and liver metastases. Following an exceptional response to FOLFIRINOX, a distal pancreatectomy (PDX No. 1, Q70P) and radiofrequency ablation of his liver metastases were performed. Two years later, a second xenograft was established (PDX No. 2, Q70LM) from new liver metastases. These liver metastases again responded to FOLFIRINOX. Finally, a third xenograft (PDX No. 3, Q70AM) was established from an abdominal wall metastasis at the time of disease

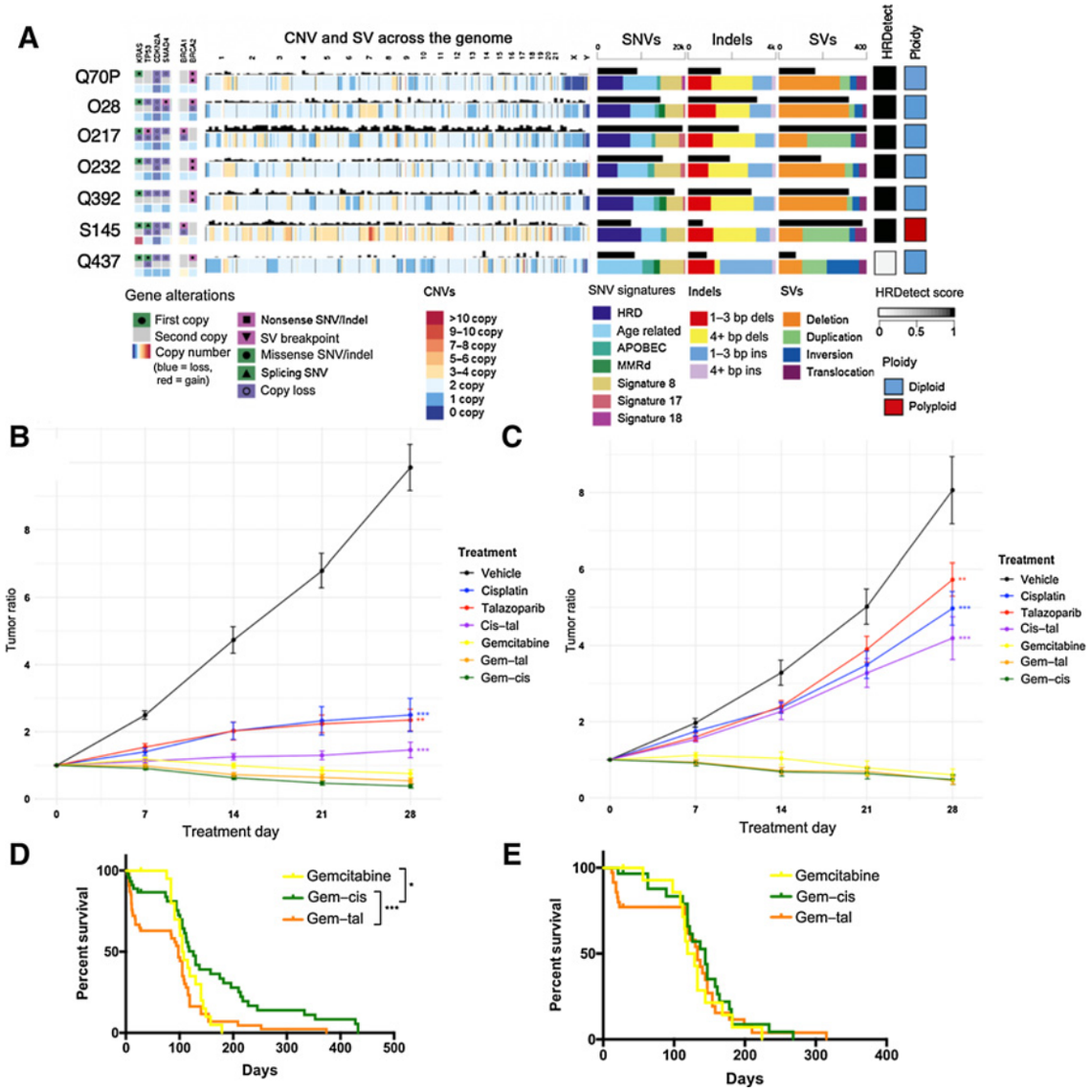

Figure 1.

Genomic characteristics of PDXs and preclinical trial outcomes. **A,** Genomic characteristics of the seven g*BRCA*-mutated PDAC cases evaluated in the preclinical trial. The first six cases have biallelic inactivation of *BRCA1* or *BRCA2*. They exhibit mutational patterns that are characteristic of HR deficiency, and have an elevated HRDetect score. In contrast, the Q437 case with monoallelic *BRCA2* inactivation lacks these genomic HRD hallmarks and has a low HRDetect score. **B** and **C,** Seven-arm preclinical trial to evaluate response of PDAC xenografts to cisplatin, talazoparib, and gemcitabine (gem) mono- and combination therapies. HRD (six unique cases, 228 mice; **B**) and HR-proficient (four unique cases, 159 mice; **C**) PDAC xenografts were treated for 28 days. For each treatment arm, the relative tumor growth (at day 28) of HRD versus HR-proficient xenografts was compared using multiple linear regression models. Gem, gemcitabine; Cis, cisplatin; Tal, talazoparib. **, $P < 0.01$; ***, $P < 0.001$. **D** and **E,** Kaplan–Meier survival curves of xenografts treated with gemcitabine mono- and combination therapies. In HRD xenografts, gemcitabine–cisplatin was associated with longer survival than gemcitabine alone and gemcitabine–talazoparib. There was no survival difference in HR-proficient xenografts. *P* values represent log-rank comparisons of Kaplan–Meier survival curves. *, $P < 0.05$; **, $P < 0.01$; ***, $P < 0.001$. Abbreviations: CNVs, copy-number variations; SNVs, single-nucleotide variants; Indels, insertions and deletions; SVs, structural variants.

progression. The patient died after two additional cycles of platinum-based therapy (gemcitabine–cisplatin).

To represent each patient by a single PDX, only the Q70P xenograft was included in the preclinical trial summarized in **Fig. 2**. However, we also performed the seven-arm preclinical trial for the two longitudinal PDXs (Q70LM and Q70AM) to evaluate their treatment sensitivities (117 mice in total). The Q70P and Q70LM xenografts showed sensitivity to cisplatin (Q70P, 4.19- vs. 11.25-fold change; $P < 0.001$ and Q70LM, 2.60 vs. 6.20; $P < 0.001$), talazoparib (Q70P, 2.26 vs. 11.25; $P < 0.001$ and Q70LM, 1.52 vs. 6.20; $P < 0.001$), and cisplatin–talazoparib (Q70P, 1.56 vs. 11.25; $P < 0.001$ and Q70LM, 1.15 vs. 6.20; $P < 0.001$) compared with vehicle, mirroring the clinically favorable response to FOLFIRINOX (**Fig. 3C**). In contrast, the Q70AM xenograft

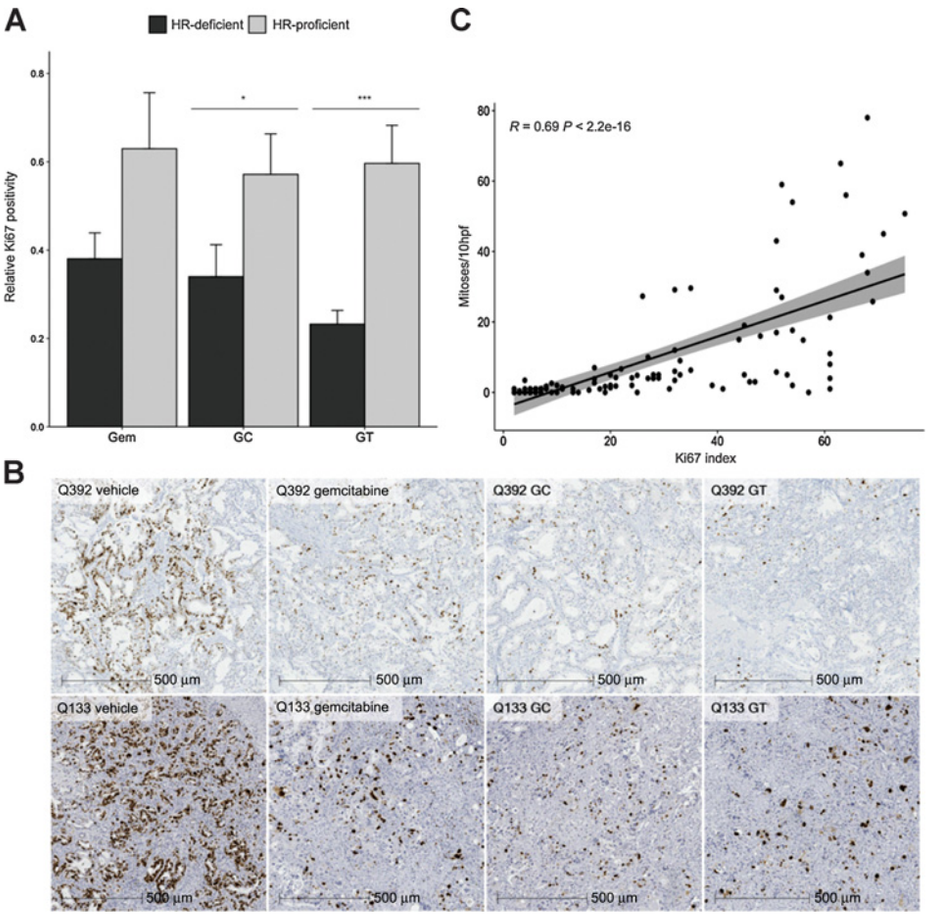

Figure 2.

Histopathologic and IHC analyses of proliferative activity in xenografts treated with gemcitabine mono- and combination therapies. **A,** Comparison of relative Ki67 positivity of HRD versus HR-proficient xenografts for each treatment arm. *, $P < 0.05$; ***, $P < 0.001$. **B,** Representative Ki67 immunostaining of Q392 (HRD) versus Q133 (HR-proficient) xenografts. GC, gemcitabine–cisplatin; GT, gemcitabine–talazoparib. **C,** Pearson correlation between absolute Ki67 positivity and mitotic activity (No. mitoses/10hpf) across all xenografts.

showed resistance to cisplatin (4.00 vs. 4.92; $P = 0.22$) and talazoparib (4.40 vs. 4.92; $P = 0.69$) monotherapy. However, this xenograft remained sensitive to cisplatin–talazoparib combination (2.29 vs. 4.92; $P < 0.001$).

To understand the mechanisms underlying this acquired resistance, we whole-genome sequenced the patient's abdominal wall metastasis (Q70AM). The germline- and somatic-inactivating *BRCA2* mutations found in the Q70P tumor were conserved in the Q70AM tumor. Both tumors had elevated HRDetect scores (>0.99) and had SNV mutational patterns dominated by SBS3 (**Fig. 4A**). However, while the Q70P tumor was diploid, the Q70AM tumor was polyploid. The liver metastasis (Q70LM) sample had insufficient cellularity for WGS, but we determined that it had also become polyploid using SNP array profiling and flow cytometric cell-cycle analysis (Supplementary Fig. S6).

A genomic scar persists in HRD xenografts treated with gemcitabine–cisplatin

To characterize changes in the genomic landscape of HRD xenografts following 28 days of treatment, we whole-genome sequenced four *BRCA2*-mutated PDAC trios. These included (i) patient primary, (ii) untreated parent PDX, and (iii) PDX treated with gemcitabine–cisplatin for 28 days, and collected at humane endpoint. We profiled xenografts from the gemcitabine–cisplatin arm, because this regimen showed the strongest and most sustained treatment response. We hypothesized that tumors that regrew following treatment cessation would have an increase in non-HRD–associated mutational signatures related to expansion of resistant subclonal populations under selective therapy pressure. In addition, to evaluate the impact of prior chemotherapy exposure, we characterized PDXs from patients that were both chemo naïve (Q392 and O232) and chemo treated (Q70P and Q70AM).

Germline and somatic *BRCA2* mutations were conserved in both the untreated parent and gemcitabine-cisplatin–treated xenografts across all trios, and there was no evidence of a reversion mutation in trial endpoint PDXs (**Fig. 4A**). Similarly, HRDetect scores remained high (>0.99) in both untreated parent and gemcitabine-cisplatin–treated xenografts. There was no significant decrease in SBS3 proportion in the gemcitabine-cisplatin–treated xenografts compared with the untreated parent xenografts (26.3% vs. 29.3%; $P = 0.89$).

Next, we evaluated the SNVs private to the gemcitabine-cisplatin–treated xenografts, and which presumably accumulated on treatment. Interestingly, these private SNVs continued to show SBS3 mutational patterns (Supplementary Fig. S7). In three of four cases, we also observed SBS3 variants private to the untreated parent xenograft, suggesting that a fraction of HRD clones may have been eradicated with gemcitabine–cisplatin. Another important observation was that the Q70AM tumor, which was chemoresistant both clinically and in the preclinical trial, retained an elevated SBS3 proportion and HRDetect score. These data suggest that a genomic HRD scar persists despite the emergence of resistance.

Gemcitabine-cisplatin–treated xenografts had a higher neoantigen load compared with their matched untreated xenograft (161 vs. 134; $P = 0.02$; **Fig. 4B**). Importantly, the Q70AM patient tumor, which

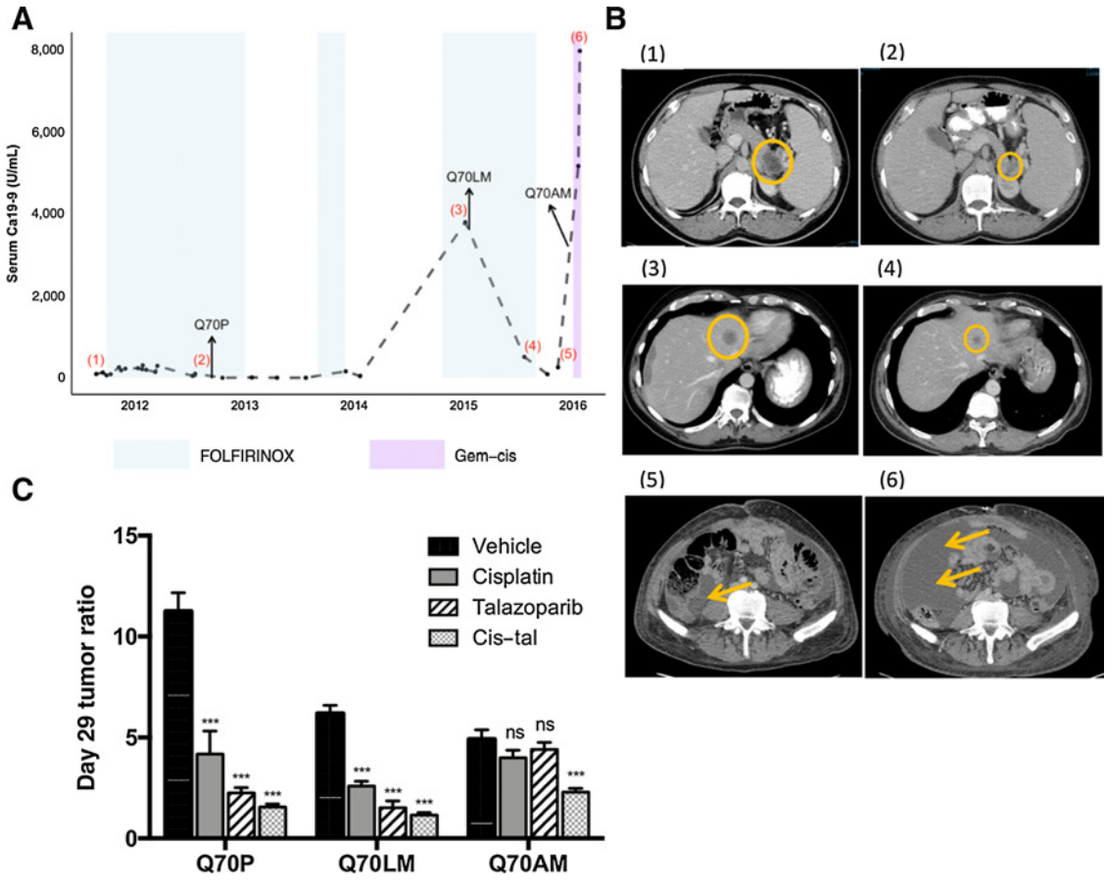

Figure 3.

Longitudinally derived xenografts from a patient with HRD PDAC (Q70) recapitulate the emergence of clinical chemoresistance. **A,** Timeline showing the evolution of serum Ca19-9 in relation to chemotherapy. Arrows indicate when the individual xenografts (Q70P, Q70LM, and Q70AM) were derived. Numbers correspond to cross-sectional imaging detailed in **B**. **B,** Representative CT scans showing chemotherapy response at various timepoints. 1–2, partial response of the pancreatic tail primary (Q70P) to FOLFIRINOX; 3–4, partial response of the liver metastases (Q70LM) to FOLFIRINOX; and 5–6, worsening of peritoneal carcinomatosis (Q70AM) on gemcitabine–cisplatin (gem–cis). **C,** Multiarm preclinical trial results for the Q70P, Q70LM, and Q70AM xenografts ($n = 117$ mice). For a given xenograft, day 29 tumor ratios were compared between each treatment arm [cisplatin, talazoparib, and cisplatin–talazoparib (cis–tal)] and vehicle. The Q70AM xenograft showed resistance to cisplatin and talazoparib alone, but remained sensitivity to cisplatin–talazoparib combination. ***, $P < 0.001$; ns, not significant.

received several additional cycles of platinum-based chemotherapy compared with the Q70P primary, exhibited a higher neoantigen load (122 vs. 82). This observation was corroborated by a higher degree of $CD8^+$ cytotoxic T-cell infiltration in the Q70AM tumor compared with the Q70P primary, albeit not to levels typically seen in mismatch repair-deficient PDAC (**Fig. 4C**).

Tumor polyploidy and low Ki67 are associated with poor response to platinum and PARPi

Among xenografts exhibiting genomic HRD hallmarks, we observed heterogeneity in individual tumor responses to cisplatin and talazoparib therapy. We searched for additional biomarkers that may be predictive of treatment response. All HRD and HRP xenografts were whole-transcriptome sequenced, and their Moffitt transcriptomic subtype was determined relative to 167 PDAC transcriptomes, 164 of which were sequenced in the COMPASS trial (ref. 35; NCT02750657). Of the eight HRD xenografts, four were basal-like, whereas the remaining four were classical. All HRP xenografts were classical (**Fig. 5A**). In addition, all HRP xenografts were profiled using an SNP array to determine their ploidy (Supplementary Fig. S6).

We performed stepwise multivariate linear regression to identify independent predictors of cisplatin (**Fig. 5B**) and talazoparib (**Fig. 5C**) response. In the cisplatin model, genomic hallmarks of HRD ($\beta = -0.478$; $P < 0.001$) and a higher Ki67 ($\beta = -0.257$; $P = 0.005$) were independently associated with better response, whereas tumor polyploidy ($\beta = 0.600$; $P < 0.001$) was associated with poor response. In the talazoparib model, HRD genomic hallmarks ($\beta = -0.299$; $P = 0.002$) and a basal-like transcriptomic subtype ($\beta = -0.442$; $P < 0.001$) were predictive of treatment response. A higher Ki67 index ($\beta = -0.192$; $P = 0.059$) was also associated with better talazoparib response, although this trend missed statistical significance. Tumor polyploidy ($\beta = 0.449$; $P < 0.001$) was again associated with poor response in the talazoparib model.

To illustrate the heterogeneity in treatment responses across individual xenografts, we performed principal component analysis followed by k-means clustering to group xenografts based on their sensitivity to cisplatin, talazoparib, and cisplatin–talazoparib (Supplementary Fig. S8). Cluster 1 identified the best responders, of which all were HRD and diploid, except Q70LM which was a polyploid HRD case with high Ki67. Cluster 2 represented the intermediate

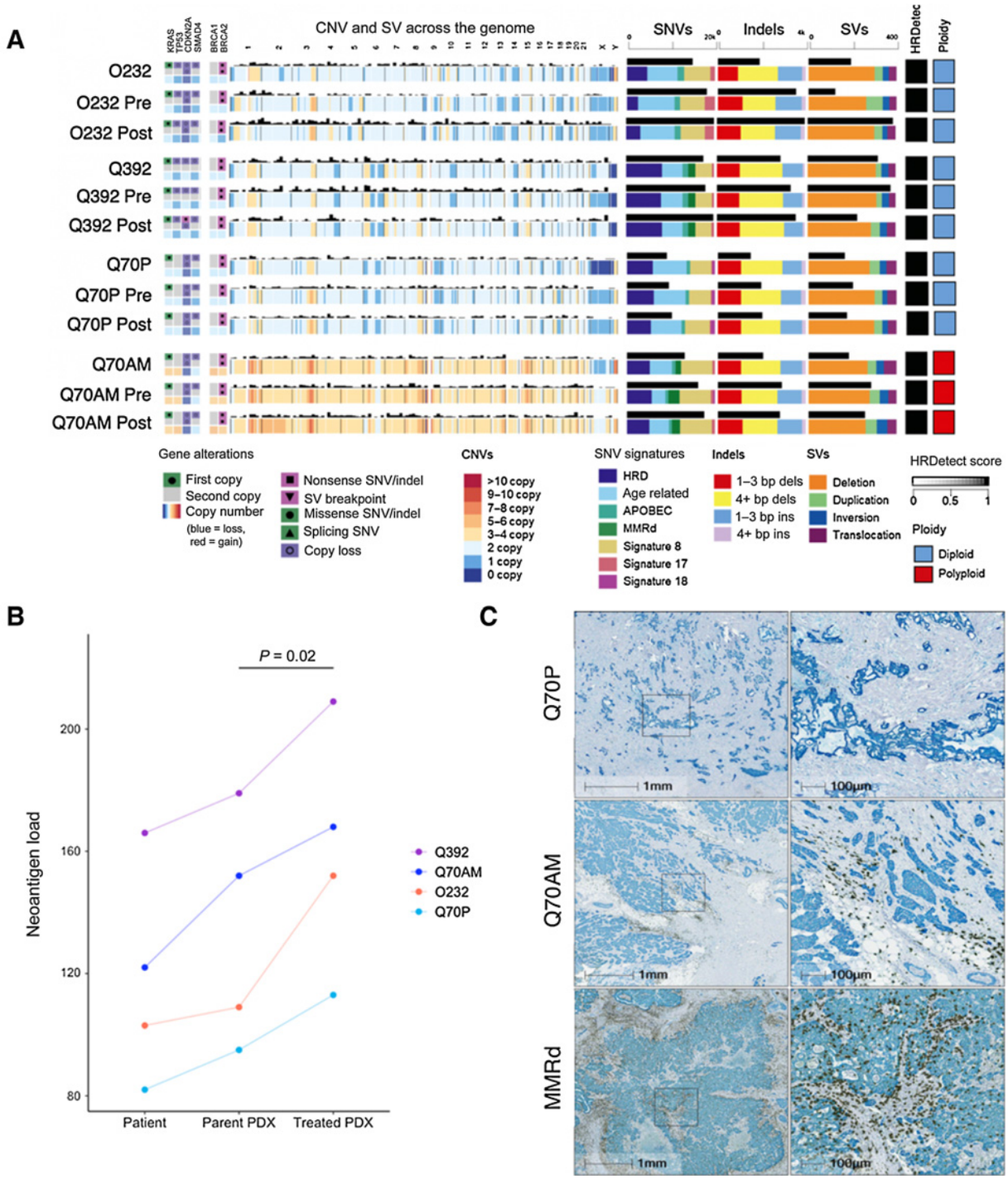

Figure 4.

WGS of four matched HRD PDAC trios to evaluate genomic changes on chemotherapy. **A,** For each case, WGS of the (i) patient primary, (ii) untreated parent PDX (pre), and (iii) PDX treated with gemcitabine–cisplatin and collected at trial endpoint (post) are shown. Germline and somatic *BRCA2* mutations were conserved in all cases. The proportion of SBS3 remained stable in the gemcitabine-cisplatin–treated xenografts. **B,** Evolution of neoantigen load between the patient, untreated parent PDX, and PDX treated with gemcitabine–cisplatin. **C,** mIHC stains showing spatial distribution of $CD8^+$ (brown) cytotoxic T cells and pan-cytokeratin$^+$ (teal) PDAC cells. Consistent with the increase in *in silico*–predicted neoantigens, there was an increase in $CD8^+$ infiltration in the Q70AM tumor compared with the Q70P. However, the $CD8^+$ infiltration remained less extensive compared with an mismatch repair (MMR)-deficient PDAC (MMRd). CNV, copy-number variation. Abbreviations: CNVs, copy-number variations; SNVs, single-nucleotide variants; Indels, insertions and deletions; SVs, structural variants.

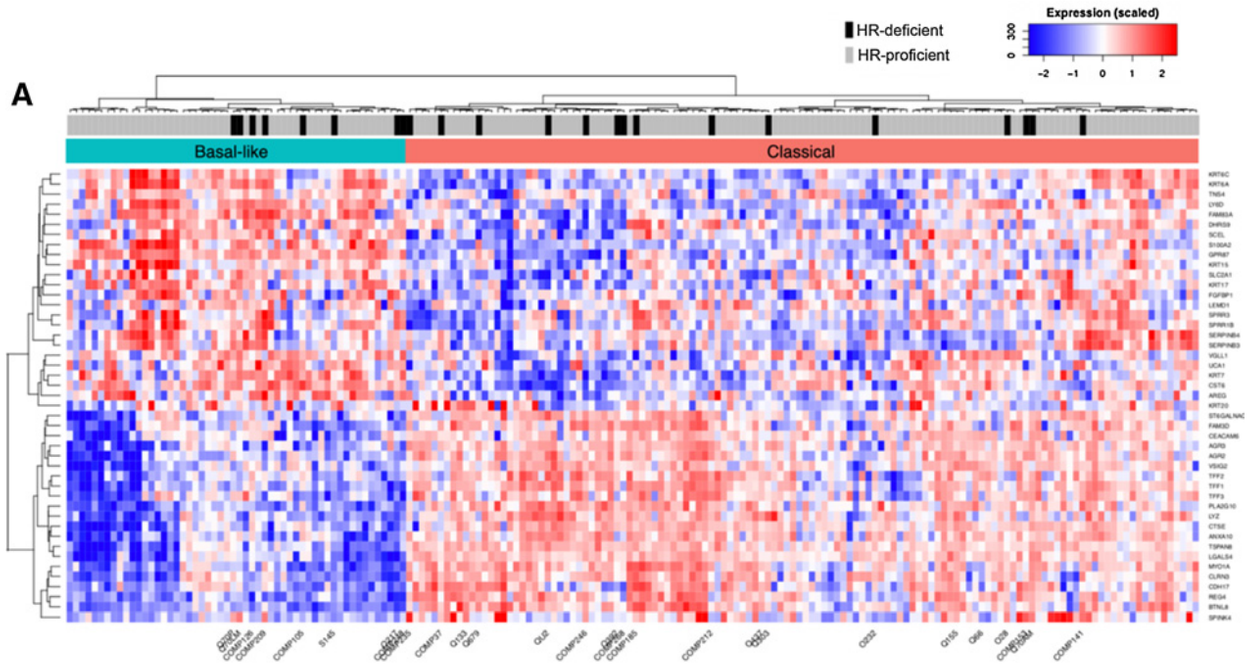

B

Variable	Standardized coefficient (β)	*P*
HRD	−0.478	<0.001
Ki67	−0.257	0.005
Polyploidy	0.600	<0.001

$R^2 = 0.578$
Excluded: Moffitt subtype, chemotherapy status

C

Variable	Standardized coefficient (β)	*P*
HRD	−0.299	0.002
Moffitt basal-like	−0.442	<0.001
Polyploidy	0.449	<0.001

$R^2 = 0.780$
Excluded: Ki67, chemotherapy status

Figure 5.

Predictive biomarkers identified on the basis of preclinical trial treatment responses. **A,** Consensus clustered heatmap of PDAC transcriptomes split by Moffitt classical and basal-like factor gene expression. The 12 xenografts evaluated in the preclinical trial were identified, and clustered relative to 167 patient PDAC transcriptomes from the COMPASS trial ($n = 164$) and non-COMPASS patients ($n = 3$). The 21 patients with HRD PDAC are indicated in black boxes. **B,** Stepwise multivariate linear regression model of predictors of cisplatin response. **C,** Stepwise multivariate linear regression model of predictors of talazoparib response.

responders, which included an HRP case (Q155), a case with monoallelic *BRCA2* inactivation and low HRDetect score (Q437), and a polyploid HRD case with high Ki67 (S145). Cluster 3 identified the xenografts with the worst treatment response, of which two were HRP, while the third was a polyploid, low Ki67, HRD case that had developed chemoresistance (Q70AM).

Across the xenografts evaluated in the preclinical trial, we observed sustained complete responses in two cases: O217 and O28. Interestingly, both were diploid, high Ki67, HRD cases from cluster 1. Both xenografts showed sustained complete responses with gemcitabine–cisplatin (median follow-up, 237 days) and cisplatin–talazoparib (median follow-up, 248 days). The O217 case also showed a sustained complete response with gemcitabine–talazoparib (median follow-up, 252 days).

Tumor polyploidy and a basal-like transcriptomic subtype are associated with worse prognosis in HRD PDAC

To evaluate the prognostic relevance of these biomarkers, we identified 21 patients with PDAC exhibiting biallelic HR gene inactivation and genomic HRD hallmarks based on WGS. In addition to the six patients whose tumors were evaluated in the preclinical trial, we also included 12 patients with HRD PDAC enrolled in the COMPASS

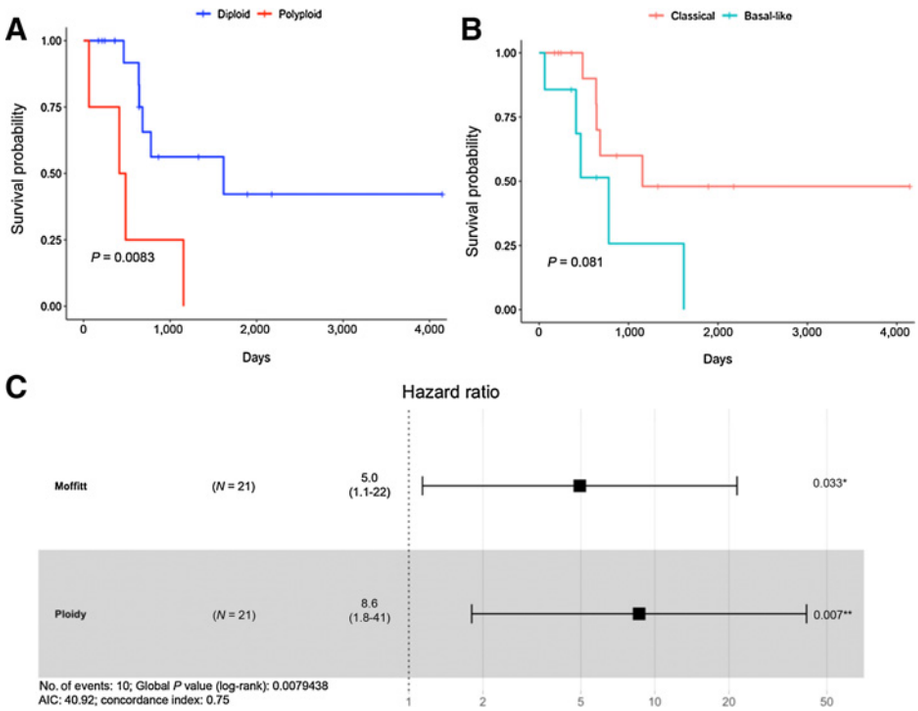

Figure 6.

Clinical outcomes of 21 patients with HRD PDAC with whole-genome and whole-transcriptomic sequencing. Kaplan–Meier survival curves are shown, stratified by tumor ploidy **(A)** and transcriptomic subtype **(B)**. *P* values represent log-rank comparisons. **C,** Multivariate Cox regression analysis with forward stepwise selection, including age, sex, stage at diagnosis, tumor ploidy, Moffitt transcriptomic subtype, and receipt of platinum-based chemotherapy. Tumor ploidy and Moffitt subtype were retained in the model and independently associated with survival. Hazard ratios and 95% confidence intervals are shown.

trial and three additional patients with HRD PDAC with whole-genome and whole-transcriptome sequencing data (Supplementary Table S2).

The mOS for all patients was 25.9 months (95% confidence interval, 0–51.9 months). Patients with polyploid tumors had shorter mOS compared with those with diploid tumors (13.8 vs. 53.9 months; $P = 0.008$; **Fig. 6A**). In addition, patients with a basal-like PDAC had shorter mOS compared with those of classical transcriptomic subtype (25.9 vs. 38.5 months; $P = 0.081$; **Fig. 6B**). We performed a multivariate Cox regression analysis with stepwise forward selection, including age, sex, stage, tumor ploidy, Moffitt transcriptomic subtype, and receipt of platinum-based chemotherapy. Tumor polyploidy (HR, 8.6; $P = 0.007$) and a basal-like transcriptomic subtype (HR, 5.0; $P = 0.033$) were independently associated with mortality (**Fig. 6C**). After adjusting for stage and sex, a basal-like subtype remained independently predictive of poor survival, whereas tumor polyploidy trended toward significance (Supplementary Fig. S9).

This clinical series included three patients who have been disease free for more than 5 years, of which two initially presented with locally advanced disease. Interestingly, all three long-term survivors had classical, diploid HRD PDAC.

GATA6:KRT17 ratio is an IHC discriminator of classical versus basal-like transcriptomic subtype

Because basal-like HRD PDAC was associated with worse prognosis, we searched for clinically practical biomarkers that could robustly predict transcriptomic subtype. Using the combined COMPASS and PDX cohorts, we compared the normalized gene expression levels (log_2CPM) of *GATA6*, *KRT17*, and *KRT81* between classical and basal-like PDAC. *GATA6* expression was significantly higher in classical tumors ($P = 2.53e\text{-}17$), whereas *KRT17* and *KRT81* expressions were significantly higher in basal-like tumors (*KRT17*, $P = 1.59e\text{-}4$ and *KRT81*, $P = 5.12e\text{-}4$; **Fig. 7A**). To validate these findings, we performed IHC staining on tissue microarrays of HRD PDAC xenografts with known Moffitt subtype. High GATA6 staining was predictive of the classical subtype with an AUC of 0.902, whereas high KRT17 staining was predictive of the basal-like subtype with an AUC of 0.828. The combination of these two markers as a GATA6:KRT17 ratio had higher predictive value than either marker alone, with an AUC of 0.971 (**Fig. 7B–D**). Using a clinically pragmatic cutoff of 1, the GATA6:KRT17 ratio had a sensitivity of 100% and a specificity of 83.3%.

We also performed mIHC to investigate the colocalization of these seemingly complementary markers. Tumors stained predominantly for one of the two markers, and only 14.9% of cells were dual positive for GATA6 and KRT17. Interestingly, we observed discrete subpopulations of $GATA6^+/KRT17^-$ and $GATA6^-/KRT17^+$ cells within the same xenograft (**Fig. 7E**). This intratumoral heterogeneity was also found in the corresponding patient tumor (Supplementary Fig. S10). Finally, we found KRT81 IHC to be a poor predictor of transcriptomic subtype, with an AUC of 0.519.

Cell lines derived from polyploid HRD PDAC xenografts are spontaneously immortal

We established primary cell cultures from eight g*BRCA*-mutated PDXs (Supplementary Table S3). Of these, three cell lines were spontaneously immortal, and could be propagated beyond 40 passages without exogenous growth factor stimulation. Interestingly, these immortal cell lines were all derived from polyploid tumors (Q70LM, Q70AM, and S145). In contrast, the five remaining primary cell cultures that were generated from diploid PDAC xenografts could only be maintained *in vitro* for a finite period, becoming senescent within two passages.

Discussion

The advent of next-generation sequencing (NGS) has accelerated the identification of molecular subtypes of PDAC with targeted therapy opportunities. However, comparing molecular-guided

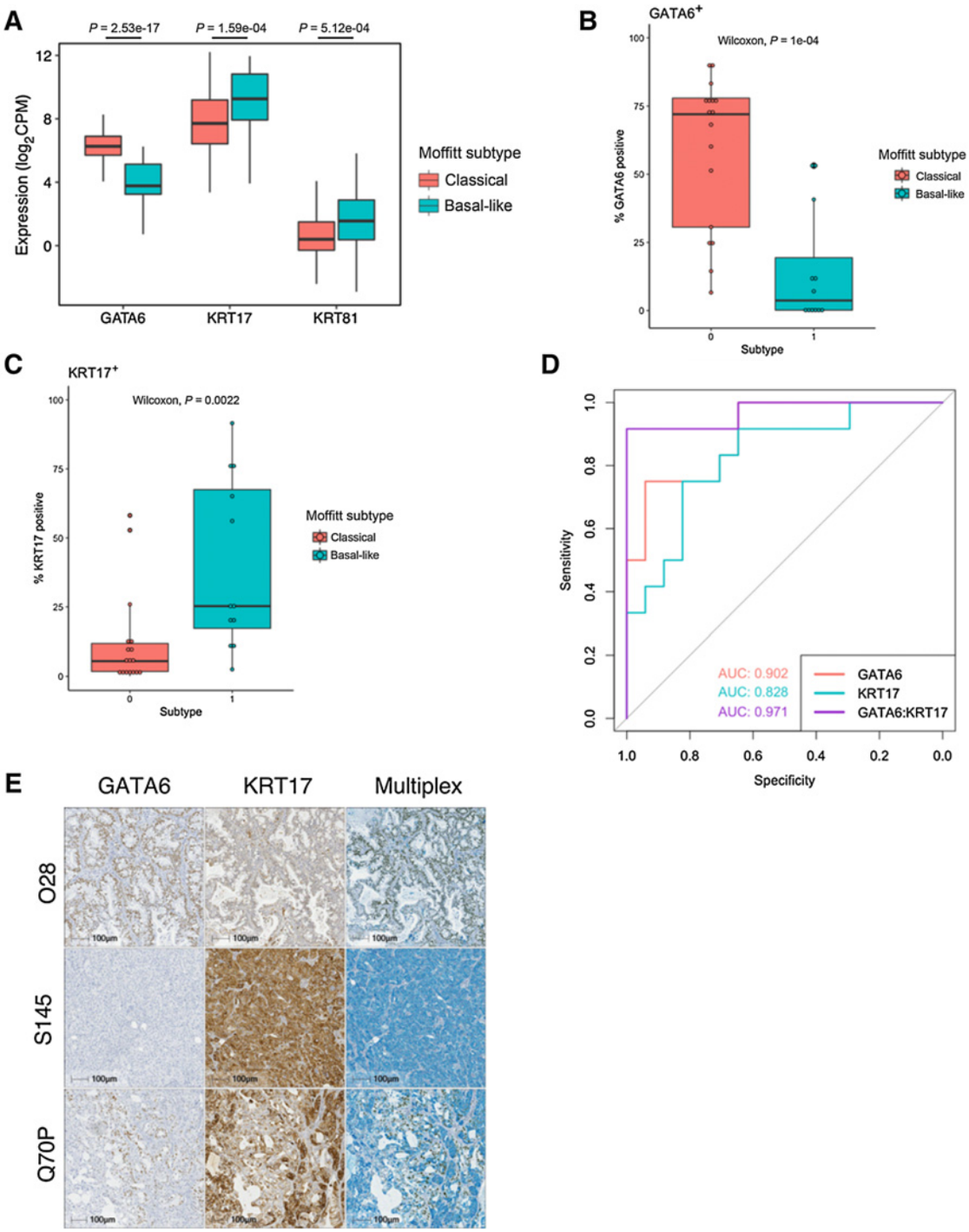

Figure 7.

IHC biomarkers of Moffitt transcriptomic subtype in HRD PDAC. **A,** TMM-normalized $\log_2$(CPM) gene expression values for *GATA6*, *KRT17*, and *KRT81* between classical and basal-like subtypes in the cohort described in Fig. 7. *GATA6* and *KRT17* were the most significantly correlated with transcriptomic subtype, and were further evaluated with IHC. **B,** Classical HRD PDAC was associated with significantly higher GATA6 positivity. GATA6 immunostaining was quantified by digital image analysis using a tumor classifier and a nuclear scoring algorithm. **C,** Basal-like HRD PDAC was associated with significantly higher KRT17 positivity, as assessed using a cytoplasmic scoring algorithm. **D,** Combining both GATA6 and KRT17 as a GATA6:KRT17 ratio had higher predictive value than either marker alone. **E,** Representative mIHC stains showing GATA6 (brown) and KRT17 (teal). Classical xenograft (O28) with predominantly $GATA6^+/KRT17^-$ cells (top). Basal-like xenograft (S145) with predominantly $GATA6^-/KRT17^+$ cells (middle). Basal-like xenograft (Q70P) with a mutually exclusive mixture of $GATA6^-/KRT17^+$ cells and $GATA6^+/KRT17^-$ cells, suggesting intratumoral heterogeneity (bottom).

treatments head-to-head using conventional clinical trial designs is impractical (36, 37). To overcome these challenges, we combined a multi-institutional patient cohort and rare PDX models to identify biomarkers underlying the therapeutic and prognostic heterogeneity of g*BRCA*-mutated PDAC, which is the most prevalent druggable PDAC subtype.

We found that biallelic inactivation of *BRCA1*/*BRCA2* was associated with mutational signatures characteristic of HR deficiency, including SBS3 and HRDetect. We showed that xenografts exhibiting HRD genomic hallmarks were preferentially sensitive to cisplatin, talazoparib, and the combination of these therapies. This has important treatment and economic implications, considering that routine germline testing is becoming standard of care in PDAC (38), and there is indication to treat *gBRCA*-mutated platinum-sensitive PDAC with PARPi based on the POLO trial (17). However, one case of monoallelic *BRCA1/BRCA2* inactivation did not exhibit HRD genomic hallmarks, and did not respond to platinum and PARPi therapies. This observation is consistent with data from breast and ovarian cancers, where monoallelically mutated tumors have been shown to exhibit low HRDetect scores and signature 3 activity, as well as poor response to platinum-based therapy (18, 34). Integration of tissue-based NGS assays (Myriad myChoice HRD, FoundationFocus $CDx_{BRCALOH}$) may help improve selection of patients for therapies targeting HR deficiency, and could be evaluated in a larger prospective cohort (39, 40).

Treatment responses to gemcitabine–cisplatin and gemcitabine–talazoparib were comparable between HRD versus HRP xenografts, and were driven by the high efficacy of gemcitabine. Considering the low clinical response rates to gemcitabine monotherapy (41), these preclinical observations highlight the limitations associated with using subcutaneous PDX models. Indeed, PDX models lack a functional immune system, do not recapitulate the tumor immune microenvironment, and present differences in intratumoral drug delivery. Thus, although PDX models allow for controlled multiarm treatment comparisons that would be difficult to perform in clinical trial settings, preclinical observations should be interpreted in the context of these limitations. Nonetheless, the combination of gemcitabine–cisplatin yielded the most durable treatment response in our preclinical trial, in addition to a significant antiproliferative effect compared with gemcitabine alone. The efficacy of gemcitabine–cisplatin was further corroborated in a recent randomized controlled trial, which showed a 65% response rate to gemcitabine–cisplatin in patients with PDAC carrying a germline *BRCA1, BRCA2*, or *PALB2* mutation (42).

Akin to clinical observations from the POLO trial and an ongoing phase II maintenance rucaparib trial (17, 43), we found heterogeneity in treatment responses among the HRD PDAC xenografts. We identified tumor polyploidy as an independent predictor of poor platinum and PARPi response. This finding is consistent with previous reports showing that polyploid cells are resistant to cytotoxic drugs (44, 45). We also found that xenografts with a higher Ki67 index had a better response to cisplatin. We identified a similar trend with talazoparib, although this did not achieve statistical significance, possibly reflecting our sample size. These observations are in concordance with studies in triple-negative breast cancer and enteropancreatic neuroendocrine tumors, in which a high Ki67 index predicts better initial responses to chemotherapy, but do not translate to improved survival. To this end, Ki67 index did not correlate with survival in our study, and its prognostic value in HRD PDAC remains unclear.

In addition, in our cohort of patients with HRD PDAC, tumor polyploidy was independently predictive of shorter survival. Importantly, this biomarker can be readily integrated into routine testing of clinical specimens using SNP genotyping assays that capture genome-wide copy-number aberrations.

Interestingly, we found that cell lines derived from polyploid g*BRCA*-mutated tumors were spontaneously immortal, whereas those generated from diploid tumors became senescent. Because spontaneous immortalization *in vitro* is not a hallmark of all cancer cells, those that become immortal may harbor aggressive features, such as polyploidy, that enable continued replication. These observations further support our finding of polyploidy as a predictive marker of poor treatment response and prognosis in g*BRCA*-mutated PDAC. Capan-1, the only published *BRCA2*-mutated pancreatic cancer cell line, has a hypotriploid genome (46). Moreover, we provide three additional polyploid g*BRCA*-mutated cell lines for *in vitro* studies, including the S145 cell line, which represents the first human *BRCA1*-mutated PDAC cell line.

Although the Q70AM xenograft was resistant to cisplatin and talazoparib monotherapies, combination of these therapies yielded a treatment response. We also observed an additive treatment benefit when combining cisplatin with talazoparib in the preclinical trial. These findings suggest a synergistic effect of combining platinum and PARPi in HRD PDAC. Importantly, talazoparib is a second-generation PARPi with higher PARP1 trapping potency and relatively high catalytic inhibition compared with earlier generation PARPis (e.g., olaparib and veliparib), which have been previously studied in PDAC. Our findings are the first to demonstrate the preclinical efficacy of talazoparib in multiple patient-derived tumors, providing motivation to evaluate talazoparib alone or in combination with platinum in a clinical trial setting.

This study is the first to investigate the implications of Moffitt transcriptomic subtypes in HRD PDAC. We identified a similar proportion of classical versus basal-like PDAC in our series compared with published cohorts (3, 35). The basal-like subtype has been associated with shorter survival and poor response to 5-fluorouracil/leucovorin (adjuvant; ref. 47) and FOLFIRINOX (metastatic first-line; ref. 35) in PDAC. In our HRD PDAC series, we found that a basal-like transcriptomic subtype was independently predictive of worse prognosis. Because there is growing evidence that discriminating between basal-like and classical transcriptomic subtypes has clinical implications not only for HRD PDAC but across PDAC, we developed a novel, clinically pragmatic two-marker IHC assay (GATA6:KRT17). We showed its ability to discriminate between the classical and basal-like subtypes with 100% and 83.3% sensitivity and specificity, respectively.

For advanced-stage g*BRCA*-mutated PDAC, retrospective series have shown a survival benefit with platinum-based therapy (7, 14, 16). In this preclinical trial, the Moffitt subtype was not predictive of response to cisplatin after adjusting for HRD genomic hallmarks. These findings suggest a hierarchy where HRD genomic features dictate platinum sensitivity over transcriptomic subtype.

Interestingly, a basal-like transcriptomic subtype was independently predictive of talazoparib sensitivity, after adjusting for HRD status. In breast cancer, "sporadic" basal-like tumors share morphologic and gene expression patterns with *BRCA1*-mutated breast cancer, suggesting that they may harbor a BRCAness phenotype (48). To this end, basal-like breast cancers have been shown to be preferentially sensitive to PARP inhibition compared with luminal cancers (49). One proposed mechanism to explain their PARPi sensitivity is that basal-like breast cancer cells may be defective in repairing oxidative DNA damage by base excision repair (50). Considering these data, and the observations from our preclinical trial, the treatment efficacy of PARPis in PDAC may not be limited to HRD cases and may include

the broader basal-like subtype. This is particularly interesting considering the chemoresistance of the basal-like subtype, and warrants further investigation.

We found that xenografts treated with gemcitabine–cisplatin retained genomic hallmarks of HRD and an elevated HRDetect score. Similarly, we demonstrated in a longitudinal study that a patient tumor that had acquired clinical chemoresistance retained a high HRDetect score. These findings suggest that HRD tumors develop a genomic scar that is the result of HRD-driven genomic mutations, and that these genomic hallmarks may not be an accurate indicator of ongoing sensitivity to HRD-targeting therapies. Thus, integrating functional assays, such as the RAD51 assay, alongside mutational signature–based biomarkers, may be a more precise strategy to select patients likely to benefit from HRD-targeted therapy (51, 52). In addition, epigenetic aberrations, such as abnormal DNA methylation, have been associated with platinum resistance (53). In preclinical studies of breast and ovarian cancer, histone deacetylase inhibitors (HDACi) have been shown to sensitize HR-proficient cells to PARPi by inducing BRCAness (54, 55). Thus, the efficacy of combination HDACi and PARPi or platinum may warrant investigation in cases with acquired resistance to HRD-targeted therapy.

Comparison of untreated versus gemcitabine-cisplatin–treated PDXs revealed SBS3 variants private to the untreated xenografts, suggesting that a fraction of HRD clones may have been eliminated with treatment. This observation provides support that therapies targeting HR deficiency can eradicate, rather than only suppress, HRD PDAC cells.

We have previously shown that HRD PDAC typically exhibits a higher mutational burden than "sporadic" PDAC, albeit lower than mismatch repair-deficient PDAC (56). The inherent susceptibility of HRD PDAC to platinum-induced DNA damage may accelerate the production of tumor-specific neoantigens, and promote an antitumor immune response. In this study, we found an increase in neoantigen load in HRD PDAC xenografts following treatment with gemcitabine–cisplatin. This observation was corroborated by a longitudinal patient case treated with FOLFIRINOX, which revealed a parallel increase in peritumoral cytotoxic T-cell infiltration that coincided with exposure to platinum-based treatment. While this increase in immune infiltration may be related to differences in immunogenicity between tumor sites, metastatic sites tend to have lower immunogenicity compared with the corresponding primary tumor (57, 58). Thus, HRD PDAC may be well-suited to treatment approaches that strategically combine or sequence platinum-based therapies, or even PARPi, with immunotherapy (59, 60).

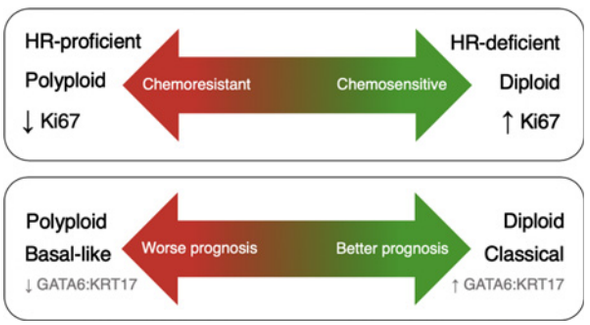

Figure 8.
Proposed schematic of predictors of chemosensitivity and prognosis in HRD PDAC.

In summary, we combined a multi-institutional patient cohort and rare preclinical models to develop a treatment sensitivity and prognostic model (**Fig. 8**) of g*BRCA*-mutated PDAC. Furthermore, we introduce a novel, clinically pragmatic two-marker assay that is predictive of transcriptomic subtype and suggest a potential role for platinum–PARPi combinations as well as immunotherapy approaches in HRD PDAC.

Disclosure of Potential Conflicts of Interest

J. Bartlett reports other from Insight Genetics, Inc. (consultancy), BioNTech AG (consultancy), Pfizer (consultancy), RNA Diagnostics Inc. (consultancy), OncoXchange/MedcomXchange Communications Inc. (consultancy), Herbert Smith French Solicitors (consultancy), OncoCyte Corporation (consultancy), Breast Cancer Society of Canada (scientific advisory board), MedcomXchange Communications Inc. (scientific advisory board, honoraria), and Oncology Education (honoraria), grants and other from NanoString Technologies, Inc. (honoraria, research funding, travel expenses) and BioTheranostics, Inc. (consultancy, honoraria, research funding, travel expenses), and grants from Thermo Fisher Scientific, Genoptix, Agendia, and Stratifyer GmbH outside the submitted work. J.M. Wilson reports grants from Government of Ontario (funding provided to the Ontario Institute for Cancer Research) during the conduct of the study. Y. Riazalhosseini reports a patent not directly connected to the submitted work regarding the use of dopamine receptor D2 (DRD2) antagonists against pancreatic cancer owned by Deutsches Krebsforschungszentrum Stiftung des öffentlichenrechts and The Royal Institution for the Advancement of Learning/McGill University. W.D. Foulkes reports grants from AstraZeneca (for assistance with interpretation of variants discovered during breast cancer susceptibility gene testing) outside the submitted work. T. Golan reports grants and personal fees from AstraZeneca (consultation fees and travel) and MSD Merck (consultation fees and travel), and personal fees from AbbVie (consultation fees and speakers bureau), Teva (consultation fees), Bayer (consultation fees), Bioline (speakers bureau), and Roche (speakers bureau) outside the submitted work. J.J. Knox reports grants from Pancreas Cancer Canada and from the Ontario Institute of Cancer Research during the conduct of the study, and grants from Merck, AstraZeneca, and Ibsen outside the submitted work. No potential conflicts of interest were disclosed by the other authors.

Authors' Contributions

Y. Wang: Conceptualization, data curation, formal analysis, investigation, visualization, methodology, writing-original draft, writing-review and editing. **J.Y.P. Park:** Conceptualization, investigation, methodology, writing-original draft, writing-review and editing. **A. Pacis:** Software, formal analysis, investigation, methodology, writing-review and editing. **R.E. Denroche:** Software, formal analysis, investigation, visualization, methodology, writing-review and editing. **G.H. Jang:** Software, formal analysis, investigation, methodology, writing-review and editing. **A. Zhang:** Software, formal analysis, investigation, visualization, methodology, writing-review and editing. **A. Cuggia:** Data curation, writing-review and editing. **C. Domecq:** Investigation, methodology, writing-review and editing. **J. Monlong:** Software, investigation, visualization, methodology, writing-review and editing. **M. Raitses-Gurevich:** Resources, data curation, writing-review and editing. **R.C. Grant:** Data curation, investigation, writing-review and editing. **A. Borgida:** Data curation, investigation, writing-review and editing. **S. Holter:** Data curation, investigation, writing-review and editing. **C. Stossel:** Resources, writing-review and editing. **S. Bu:** Investigation, methodology, writing-review and editing. **M. Masoomian:** Investigation, writing-review and editing. **I. Lungu:** Resources, methodology, writing-review and editing. **J. Bartlett:** Resources, methodology, writing-review and editing. **J.M. Wilson:** Resources, funding acquisition, project administration, writing-review and editing. **Z.-H. Gao:** Supervision, investigation, methodology, writing-review and editing. **Y. Riazalhosseini:** Supervision, investigation, methodology, writing-review and editing. **J. Asselah:** Resources, writing-review and editing. **N. Bouganim:** Resources, writing-review and editing. **T. Cabrera:** Resources, writing-review and editing. **L.-M. Boucher:** Resources, writing-review and editing. **D. Valenti:** Resources, writing-review and editing. **J. Biagi:** Resources, funding acquisition, writing-review and editing. **C.M.T. Greenwood:** Supervision, methodology, writing-review and editing. **P. Polak:** Resources, supervision, writing-review and editing. **W.D. Foulkes:** Resources, supervision, writing-review and editing. **T. Golan:** Resources, funding acquisition, writing-review and editing. **G.M. O'Kane:** Resources, data curation, investigation, writing-review and editing. **S.E. Fischer:** Resources, investigation, project administration, writing-review and editing. **J.J. Knox:** Resources,

supervision, funding acquisition, writing-review and editing. **S. Gallinger:** Conceptualization, resources, supervision, funding acquisition, project administration, writing-review and editing. **G. Zogopoulos:** Conceptualization, resources, supervision, funding acquisition, writing-original draft, project administration, writing-review and editing.

Acknowledgments

This work was supported through funding provided by the Cancer Research Society/Ganotec-Marc-André Pigeon Memorial Fund (grant no. 20280), the Terry Fox Research Institute (project no. 1078), and the Pancreatic Cancer Canada Foundation. This study was conducted with the support of the Ontario Institute for Cancer Research (PanCuRx Translational Research Initiative) through funding provided by the Government of Ontario, the Wallace McCain Centre for Pancreatic Cancer supported by the Princess Margaret Cancer Foundation, and the Canadian Cancer Society Research Institute. This study was also supported by charitable donations from the Canadian Friends of the Hebrew University (Alex U. Soyka). Y. Wang was supported by a Vanier Canada Graduate Scholarship, the Fonds de recherche du Québec – Santé/Ministère de la Santé et des Services sociaux training program, and the McGill University Surgical-Scientist Program. Y. Riazalhosseini is a research scholar of the Fonds de recherche du Québec – Santé. G.M. O'Kane was supported by the Lewitt fellowship. J.J. Knox is the recipient of the Wilfred G. Lewitt Chair in Pancreatic Cancer Research. S. Gallinger is the recipient of an Investigator Award from the Ontario Institute for Cancer Research. G. Zogopoulos is a clinical research scholar of the Fonds de recherche du Québec – Santé. We acknowledge the contributions of Crystal Haigh, HPB Surgical and Medical Oncology, Pathology and Interventional Radiology at the McGill University Health Centre. We also acknowledge the contributions of team members at the Ontario Institute for Cancer Research within the Genomics & Bioinformatics platform (genomics.oicr.on.ca), as well as the contributions of Dianne Chadwick, Sheng-Ben Liang, and Sana Sagri at the University Health Network Oncology Biobank.

The costs of publication of this article were defrayed in part by the payment of page charges. This article must therefore be hereby marked *advertisement* in accordance with 18 U.S.C. Section 1734 solely to indicate this fact.

Received April 18, 2020; revised June 24, 2020; accepted August 3, 2020; published first August 14, 2020.

References

1. Siegel RL, Miller KD, Jemal A. Cancer statistics, 2019. CA Cancer J Clin 2019;69:7–34.
2. Rawla P, Thandra KC, Sunkara T. Pancreatic cancer and obesity: epidemiology, mechanism, and preventive strategies. Clin J Gastroenterol 2019;12:285–91.
3. Moffitt RA, Marayati R, Flate EL, Volmar KE, Loeza SGH, Hoadley KA, et al. Virtual microdissection identifies distinct tumor- and stroma-specific subtypes of pancreatic ductal adenocarcinoma. Nat Genet 2015;47:1168–78.
4. Bailey P, Chang DK, Nones K, Johns AL, Patch A-M, Gingras M-C, et al. Genomic analyses identify molecular subtypes of pancreatic cancer. Nature 2016;531:47–52.
5. Collisson EA, Sadanandam A, Olson P, Gibb WJ, Truitt M, Gu S, et al. Subtypes of pancreatic ductal adenocarcinoma and their differing responses to therapy. Nat Med 2011;17:500–3.
6. Waddell N, Pajic M, Patch A-M, Chang DK, Kassahn KS, Bailey P, et al. Whole genomes redefine the mutational landscape of pancreatic cancer. Nature 2015;518:495–501.
7. Smith AL, Wong C, Cuggia A, Borgida A, Holter S, Hall A, et al. Reflex testing for germline BRCA1, BRCA2, PALB2, and ATM mutations in pancreatic cancer: mutation prevalence and clinical outcomes from two canadian research registries. JCO Precision Oncology 2018;2:1–16.
8. Holter S, Borgida A, Dodd A, Grant R, Semotiuk K, Hedley D, et al. Germline BRCA mutations in a large clinic-based cohort of patients with pancreatic adenocarcinoma. J Clin Oncol 2015;33:3124–9.
9. Chen C-C, Feng W, Lim PX, Kass EM, Jasin M. Homology-directed repair and the role of BRCA1, BRCA2, and related proteins in genome integrity and cancer. Annu Rev Cancer Biol 2018;2:313–36.
10. Andrei A-Z, Hall A, Smith AL, Bascuñana C, Malina A, Connor A, et al. Increased in vitro and in vivo sensitivity of BRCA2-associated pancreatic cancer to the poly(ADP-ribose) polymerase-1/2 inhibitor BMN 673. Cancer Lett 2015;364:8–16.
11. Lord CJ, Ashworth A. The DNA damage response and cancer therapy. Nature 2012;481:287–94.
12. Lord CJ, Ashworth A. PARP inhibitors: synthetic lethality in the clinic. Science 2017;355:1152–8.
13. Lee J-M, Ledermann JA, Kohn EC. PARP inhibitors for BRCA1/2 mutation-associated and BRCA-like malignancies. Ann Oncol 2014;25:32–40.
14. Golan T, Kanji ZS, Epelbaum R, Devaud N, Dagan E, Holter S, et al. Overall survival and clinical characteristics of pancreatic cancer in BRCA mutation carriers. Br J Cancer 2014;111:1132–8.
15. Rebelatto TF, Falavigna M, Pozzari M, Spada F, Cella CA, Laffi A, et al. Should platinum-based chemotherapy be preferred for germline BReast CAncer genes (BRCA) 1 and 2-mutated pancreatic ductal adenocarcinoma (PDAC) patients? A systematic review and meta-analysis. Cancer Treat Rev 2019;80:101895.
16. Pishvaian MJ, Blais EM, Brody JR, Rahib L, Lyons E, De Arbeloa P, et al. Outcomes in patients with pancreatic adenocarcinoma with genetic mutations in DNA damage response pathways: results from the know your tumor program. JCO Precision Oncology 2019;3:1–10.
17. Golan T, Hammel P, Reni M, Van Cutsem E, Macarulla T, Hall MJ, et al. Maintenance olaparib for germline BRCA-mutated metastatic pancreatic cancer. N Engl J Med 2019;381:317–27.
18. Maxwell KN, Wubbenhorst B, Wenz BM, De Sloover D, Pluta J, Emery L, et al. BRCA locus-specific loss of heterozygosity in germline BRCA1 and BRCA2 carriers. Nat Commun 2017;8:319.
19. Patch A-M, Christie EL, Etemadmoghadam D, Garsed DW, George J, Fereday S, et al. Whole-genome characterization of chemoresistant ovarian cancer. Nature 2015;521:489–94.
20. Sakai W, Swisher EM, Karlan BY, Agarwal MK, Higgins J, Friedman C, et al. Secondary mutations as a mechanism of cisplatin resistance in BRCA2-mutated cancers. Nature 2008;451:1116–20.
21. Norquist B, Wurz KA, Pennil CC, Garcia R, Gross J, Sakai W, et al. Secondary somatic mutations restoring BRCA1/2 predict chemotherapy resistance in hereditary ovarian carcinomas. J Clin Oncol 2011;29:3008–15.
22. Denroche RE, Mullen L, Timms L, Beck T, Yung CK, Stein L, et al. A cancer cell-line titration series for evaluating somatic classification. BMC Res Notes 2015;8:823–10.
23. Davies H, Glodzik D, Morganella S, Yates LR, Staaf J, Zou X, et al. HRDetect is a predictor of BRCA1 and BRCA2 deficiency based on mutational signatures. Nat Med 2017;23:517–25.
24. Alexandrov LB, Nik-Zainal S, Wedge DC, Aparicio SAJR, Behjati S, Biankin AV, et al. Signatures of mutational processes in human cancer. Nature 2013;500:415–21.
25. Bolger AM, Lohse M, Usadel B. Trimmomatic: a flexible trimmer for Illumina sequence data. Bioinformatics 2014;30:2114–20.
26. Dobin A, Davis CA, Schlesinger F, Drenkow J, Zaleski C, Jha S, et al. STAR: ultrafast universal RNA-seq aligner. Bioinformatics 2013;29:15–21.
27. Ahdesmäki MJ, Gray SR, Johnson JH, Lai Z. Disambiguate: an open-source application for disambiguating two species in next generation sequencing data from grafted samples. F1000Res 2016;5:2741.
28. Anders S, Pyl PT, Huber W. HTSeq–a Python framework to work with high-throughput sequencing data. Bioinformatics 2015;31:166–9.
29. Robinson MD, McCarthy DJ, Smyth GK. edgeR: a bioconductor package for differential expression analysis of digital gene expression data. Bioinformatics 2010;26:139–40.
30. Ritchie ME, Phipson B, Wu D, Hu Y, Law CW, Shi W, et al. limma powers differential expression analyses for RNA-sequencing and microarray studies. Nucleic Acids Res 2015;43:e47–7.
31. Agorku DJ, Tomiuk S, Klingner K, Wild S, Rüberg S, Zatrieb L, et al. Depletion of mouse cells from human tumor xenografts significantly improves downstream analysis of target cells. J Vis Exp 2016;29:54259.
32. Nunez R. DNA measurement and cell cycle analysis by flow cytometry. Curr Issues Mol Biol 2001;3:67–70.
33. Van Loo P, Nordgard SH, Lingjærde OC, Russnes HG, Rye IH, Sun W, et al. Allele-specific copy number analysis of tumors. Proc Natl Acad Sci U S A 2010;107:16910–5.

34. Polak P, Kim J, Braunstein LZ, Karlic R, Haradhavala NJ, Tiao G, et al. A mutational signature reveals alterations underlying deficient homologous recombination repair in breast cancer. Nat Genet 2017;49:1476–86.
35. Aung KL, Fischer SE, Denroche RE, Jang GH, Dodd A, Creighton S, et al. Genomics-driven precision medicine for advanced pancreatic cancer: early results from the COMPASS trial. Clin Cancer Res 2018;24:1344–54.
36. Ersek JL, Black LJ, Thompson MA, Kim ES. Implementing precision medicine programs and clinical trials in the community-based oncology practice: barriers and best practices. Am Soc Clin Oncol Educ Book 2018;38:188–96.
37. Garralda E, Dienstmann R, Piris-Giménez A, Braña I, Rodon J, Tabernero J. New clinical trial designs in the era of precision medicine. Mol Oncol 2019;13:549–57.
38. Tempero MA. NCCN guidelines updates: pancreatic cancer. J Natl Compr Canc Netw 2019;17:603–5.
39. Coleman RL, Oza AM, Lorusso D, Aghajanian C, Oaknin A, Dean A, et al. Rucaparib maintenance treatment for recurrent ovarian carcinoma after response to platinum therapy (ARIEL3): a randomised, double-blind, placebo-controlled, phase 3 trial. Lancet 2017;390:1949–61.
40. Telli ML, Timms KM, Reid J, Hennessy B, Mills GB, Jensen KC, et al. Homologous recombination deficiency (HRD) score predicts response to platinum-containing neoadjuvant chemotherapy in patients with triple-negative breast cancer. Clin Cancer Res 2016;22:3764–73.
41. Burris HA, Moore MJ, Andersen J, Green MR, Rothenberg ML, Modiano MR, et al. Improvements in survival and clinical benefit with gemcitabine as first-line therapy for patients with advanced pancreas cancer: a randomized trial. J Clin Oncol 1997;15:2403–13.
42. O'Reilly EM, Lee JW, Zalupski M, Capanu M, Park J, Golan T, et al. Randomized, multicenter, phase II trial of gemcitabine and cisplatin with or without veliparib in patients with pancreas adenocarcinoma and a germline BRCA/PALB2 mutation. J Clin Oncol 2020;38:1378–88.
43. Binder KAR, Mick R, O 039 Hara M, Teitelbaum U, Karasic T, Schneider C, et al. Abstract CT234: a phase II, single arm study of maintenance rucaparib in patients with platinum-sensitive advanced pancreatic cancer and a pathogenic germline or somatic mutation in *BRCA1, BRCA2*; or *PALB2*. Cancer Res 2019;79:CT234.
44. Lee AJX, Endesfelder D, Rowan AJ, Walther A, Birkbak NJ, Futreal PA, et al. Chromosomal instability confers intrinsic multidrug resistance. Cancer Res 2011;71:1858–70.
45. Passerini V, Ozeri-Galai E, de Pagter MS, Donnelly N, Schmalbrock S, Kloosterman WP, et al. The presence of extra chromosomes leads to genomic instability. Nat Commun 2016;7:10754–12.
46. Barber LJ, Rosa JM, Kozarewa I, Fenwick K, Assiotis I, Mitsopoulos C, et al. Comprehensive genomic analysis of a BRCA2 deficient human pancreatic cancer. PLoS One 2011;6:e21639.
47. Martinelli P, Carrillo-de Santa Pau E, Cox T, Sainz B, Dusetti N, Greenhalf W, et al. GATA6 regulates EMT and tumour dissemination, and is a marker of response to adjuvant chemotherapy in pancreatic cancer. Gut 2017;66:1665–76.
48. De Summa S, Pinto R, Sambiasi D, Petriella D, Paradiso V, Paradiso A, et al. BRCAness: a deeper insight into basal-like breast tumors. Ann Oncol 2013;24:viii13–viii21.
49. Hastak K, Alli E, Ford JM. Synergistic chemosensitivity of triple-negative breast cancer cell lines to poly(ADP-Ribose) polymerase inhibition, gemcitabine, and cisplatin. Cancer Res 2010;70:7970–80.
50. Alli E, Sharma VB, Sunderesakumar P, Ford JM. Defective repair of oxidative DNA damage in triple-negative breast cancer confers sensitivity to inhibition of poly(ADP-ribose) polymerase. Cancer Res 2009;69:3589–96.
51. Castroviejo-Bermejo M, Cruz C, Llop-Guevara A, Gutiérrez-Enríquez S, Ducy M, Ibrahim YH, et al. A RAD51 assay feasible in routine tumor samples calls PARP inhibitor response beyond BRCA mutation. EMBO Mol Med 2018;10:e9172.
52. Cruz C, Castroviejo-Bermejo M, Gutiérrez-Enríquez S, Llop-Guevara A, Ibrahim YH, Gris-Oliver A, et al. RAD51 foci as a functional biomarker of homologous recombination repair and PARP inhibitor resistance in germline BRCA-mutated breast cancer. Ann Oncol 2018;29:1203–10.
53. Wei SH, Balch C, Paik HH, Kim Y-S, Baldwin RL, Liyanarachchi S, et al. Prognostic DNA methylation biomarkers in ovarian cancer. Clin Cancer Res 2006;12:2788–94.
54. Ha K, Fiskus W, Choi DS, Bhaskara S, Cerchietti L, Devaraj SGT, et al. Histone deacetylase inhibitor treatment induces "BRCAness" and synergistic lethality with PARP inhibitor and cisplatin against human triple negative breast cancer cells. Oncotarget 2014;5:5637–50.
55. Yin L, Liu Y, Peng Y, Peng Y, Yu X, Gao Y, et al. PARP inhibitor veliparib and HDAC inhibitor SAHA synergistically co-target the UHRF1/BRCA1 DNA damage repair complex in prostate cancer cells. J Exp Clin Cancer Res 2018;37:153–14.
56. Connor AA, Denroche RE, Jang GH, Timms L, Kalimuthu SN, Selander I, et al. Association of distinct mutational signatures with correlates of increased immune activity in pancreatic ductal adenocarcinoma. JAMA Oncol 2017;3:774–83.
57. Blando J, Sharma A, Higa MG, Zhao H, Vence L, Yadav SS, et al. Comparison of immune infiltrates in melanoma and pancreatic cancer highlights VISTA as a potential target in pancreatic cancer. Proc Natl Acad Sci U S A 2019;116:1692–7.
58. Szekely B, Bossuyt V, Li X, Wali VB, Patwardhan GA, Frederick C, et al. Immunological differences between primary and metastatic breast cancer. Ann Oncol 2018;29:2232–9.
59. Strickland KC, Howitt BE, Shukla SA, Rodig S, Ritterhouse LL, Liu JF, et al. Association and prognostic significance of BRCA1/2-mutation status with neoantigen load, number of tumor-infiltrating lymphocytes and expression of PD-1/PD-L1 in high grade serous ovarian cancer. Oncotarget 2016;7:13587–98.
60. Gilmore E, McCabe N, Kennedy RD, Parkes EE. DNA repair deficiency in breast cancer: opportunities for immunotherapy. J Oncol 2019;2019:4325105–14.